Electronic Supplementary Information

Revealing electronic features governing hydrolysis of cephalosporins in the active site of the L1 metallo-β-lactamase

Elena O. Levina,[a,b] Maria G. Khrenova,[a,c*] Andrey A. Astakhov[a,d] and Vladimir G. Tsirelson[a,e]

[a] *Federal Research Centre "Fundamentals of Biotechnology" of the Russian Academy of Sciences, Moscow, Russia*

[b] *Moscow Institute of Physics and Technology, Dolgoprudny, Russia*

[c] *Lomonosov Moscow State University, Moscow, Russia*

[d] *Joint Institute for Nuclear Research, Dubna, Russia*

[e] *Mendeleev University of Chemical Technology of Russia, Moscow, Russia*

[*] *Corresponding author*: Maria G. Khrenova, e-mail: khrenova.maria@gmail.com

S1. Computational details of descriptor calculations

Computational protocol for condensed linear response kernel and delocalization tensor analysis, which require the information about virtual orbitals, was as follows. The single point Firefly QC[1] computations were carried out for PES stationary point structures, obtained by QM/MM method. The protein and solute surrounding were treated by effective fragment potential scheme,[2,3] i.e. the environmental effects on the cephalosporins and L1 MβL active site were included explicitly. The Molden program package[4] was used to convert obtained files to Multiwfn program format. To reduce computational costs the integration of linear response kernel was carried out using Becke's numerical integration scheme.[5] We used atomic radii deduced from the Cambridge Structural Database data[6] modified by Lu.[7] Also the results are based on the computations of cephalosporin and active cite systems without protein and solute surrounding. The accuracy of integration was evaluated as deviation of atomic overlap matrix sum (for all atoms) to identity matrix, divided by number of atoms. Obtained errors do not exceed few per thousand. Note that calculations with the explicitly included effects of protein and solute surrounding gave lower integration accuracy. However, the character of computed dependencies of condensed linear response kernel elements on the number of atoms of the C_4-C_3-R_2 fragment (see Section 3.3) consists with that obtained for the cephalosporin and active cite complexes without account for protein and solute surrounding.

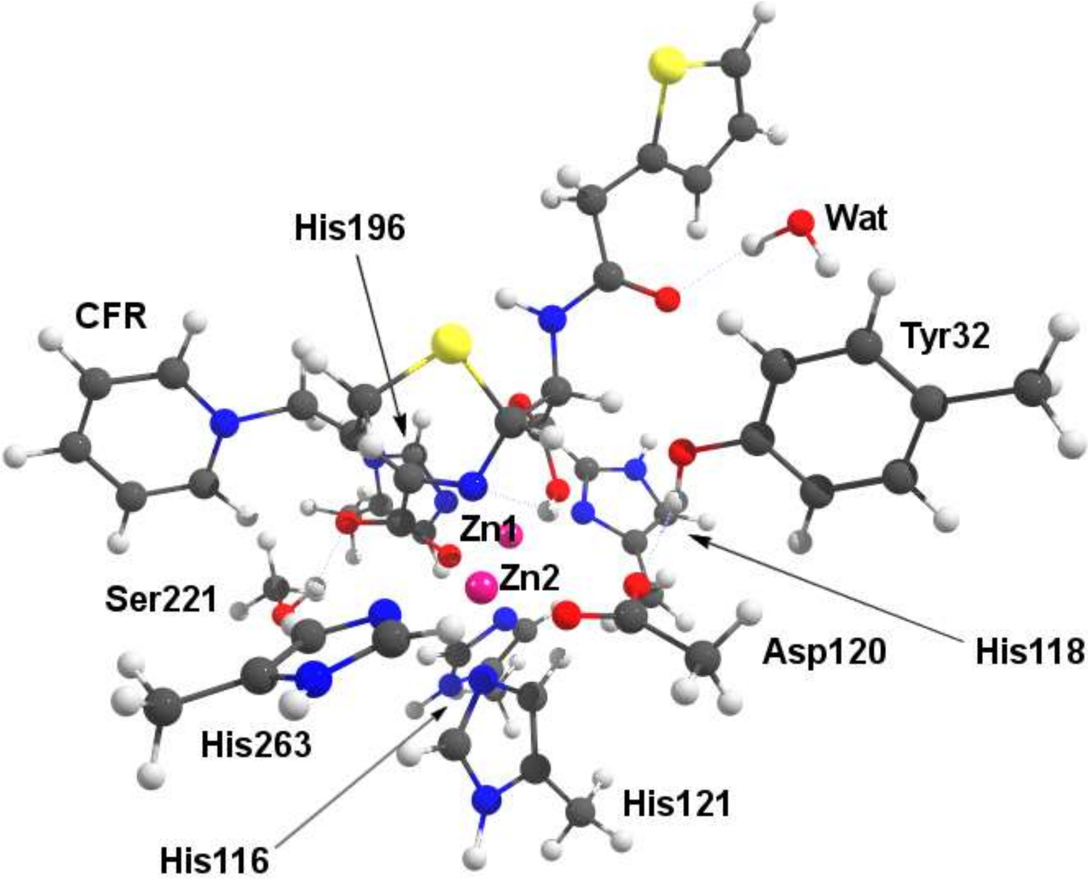

Fig. S1 QM subsystem of TS complex for CFR hydrolyzed by L1 MβL. The red, blue, yellow, gray and white spheres represent oxygen, sulfur, nitrogen, carbon and hydrogen atoms, respectively, while magenta spheres represent Zn^{2+} ions.

S2. Short Review of Bonding Descriptors

There are several approaches for chemical bonding analysis making use of some real-space distributed descriptors.[8–23] Some of them provide information about the electron-density features in nearest region around of some spatial point in the molecular system. It is, for example, the bond **e*llipticity of electron densit*y**, $\varepsilon = \frac{\lambda_1}{\lambda_2} - 1$,[24] which is a measure of the deviation of electron density along the bond path from axial symmetry (λ_1 and λ_2 are negative eigenvalues of Hesse matrix of electron density ($|\lambda_2| < |\lambda_1|$); it indicates existence of the π character of chemical bonds.[24–29] The other carries information about mutual influence of electrons in spatially remote regions and reveal the electron exchange and Coulomb correlation effects. The non-local descriptors used in this study are the source function,[8,30] Fermi hole,[9,31] electron delocalization indices,[32] delocalization tensor[10] and condensed linear response kernel.[33] They are briefly characterized below.

Source (or influence) function reveals the distant self-influence encoded in electron density. For the electron density at a reference point $\boldsymbol{r}$, it is given by contributions of a local density sources $G(\boldsymbol{r},\boldsymbol{r}') = -\frac{1}{4\pi}\frac{\nabla^2\rho(\boldsymbol{r}')}{|\boldsymbol{r}-\boldsymbol{r}\prime|}$, operating at all other points $\boldsymbol{r}'$:[8,30]

$$\rho(\boldsymbol{r}) = \int G(\boldsymbol{r},\boldsymbol{r}')d\boldsymbol{r}' \,, \tag{1}$$

$G(\boldsymbol{r},\boldsymbol{r}')$ represents the influence of ρ curvature in point $\boldsymbol{r}'$ on electron density at the point $\boldsymbol{r}$. Decomposing (1) in atomic contributions

$$\rho(\boldsymbol{r}) = -\frac{1}{4\pi}\sum_{i}^{N}\int_{\Omega_i}\frac{\nabla^2\rho(\boldsymbol{r}')}{|\boldsymbol{r}-\boldsymbol{r}'|}d\boldsymbol{r}' = \sum_{\boldsymbol{i}}^{\boldsymbol{N}} SF(\boldsymbol{r},\,\Omega_i) \tag{2}$$

we arrive at atomic **source function,** $SF(\boldsymbol{r},\,\Omega_i)$, where Ω_i is QTAIM zero-flux atomic basin in the molecular system. SF expresses the influence of *i* atom on the electron density at reference point ***r***. Atom yielding the positive contribution acts like a “source” of the density field, while negative contribution means that atom acts like a “sink”. The percentage form of SF is[34]

$$SF(\boldsymbol{r},\,\Omega_i),\% = \frac{SF(\boldsymbol{r},\,\Omega_i)}{\rho(\boldsymbol{r})}\cdot 100\,\% \tag{3}$$

Source function allows to examine a mutual influence of any atoms connected or not by the bond paths. It is widely applied to examine multicenter atomic interactions,[35] chemical transferability of the atomic groups in a molecule,[30,36] hydrogen bonding[37,38,39] and features of non-covalent bonding in the prototypes of bioactive molecules.[39,40]

The electron pair density, $\rho_2(\boldsymbol{r},\boldsymbol{r}')$,[41] describes probability of simultaneous finding of two electrons in points $\boldsymbol{r}$ and $\boldsymbol{r}'$. The difference between correlated pair density $\rho_2(\boldsymbol{r},\boldsymbol{r}')$ and formally uncorrelated distribution of electrons $\rho(\boldsymbol{r})\rho(\boldsymbol{r}')$ is caused by the electron exchange and correlation effects. They are described by the exchange-correlation hole

$$h_{xc}(\boldsymbol{r},\boldsymbol{r}') = \frac{\rho_2(\boldsymbol{r},\boldsymbol{r}')}{\rho(\boldsymbol{r})} - \frac{\rho(\boldsymbol{r})\rho(\boldsymbol{r}')}{\rho(\boldsymbol{r})} = P(\boldsymbol{r}'|\boldsymbol{r}) - \rho(\boldsymbol{r}'), \tag{4}$$

where $P(\boldsymbol{r}'|\boldsymbol{r})$ is the conditional probability density, i.e. the probability of finding one electron at a point $\boldsymbol{r}'$ while the reference electron is fixed in a position $\boldsymbol{r}$. In the non-interacting electron system, Coulomb correlation is ignored, and expression (4) is called the **Fermi (**or exchange) **hole**, $h_x(\boldsymbol{r},\boldsymbol{r}')$.[42,43] It expresses the decrease in probability of finding electron with spin σ at a point $\boldsymbol{r}'$ while the reference electron of the same spin is fixed in a position $\boldsymbol{r}$. It is a direct consequence of the Pauli Exclusion Principle caused by requirement for the manyelectron wave function to be antisymmetric.[31] An electron moving in space carries its Fermi hole, and if the Fermi hole is localized in some region of space, so the electron does.[9] In case of closed-shell system it also can be interpreted as a measure of electron pair localization.

The information about localization of electrons contained in the Fermi hole can be compactly represented via ***localization and delocalization indices,*** scalar atomic characteristics integrated over atomic basins. The integration over a single atomic basin *A*, gives localization index:[32,44]

$$\lambda_A = -\int_{\Omega_A} d\boldsymbol{r} \int_{\Omega_A} d\boldsymbol{r}' \rho(\boldsymbol{r}) h_x(\boldsymbol{r},\boldsymbol{r}') \tag{5}$$

It describes the number of electrons which are removed from the basin *A* due to the Pauli principle. Hence it also indicates the number of electron pairs which are remained in this basin, i.e. describe the localization of electrons.

The electron delocalization index shows the number of electron pairs spreading out between basins of *A* and *B* atoms:[32,45]

$$\delta_{AB} = -\frac{1}{2}\int_{\Omega_A} d\boldsymbol{r} \int_{\Omega_B} d\boldsymbol{r}' \rho(\boldsymbol{r}) h_x(\boldsymbol{r},\boldsymbol{r}') \tag{6}$$

The sum of localization indices of all atoms and delocalization indices between all pairs of atoms gives total number of electrons in a system and these indices are used to characterize the type of chemical bonding or reaction activity of compounds.

The Fermi hole and the localization and delocalization indices evaluate average spreading of electrons in all possible directions. The **delocalization tensor**[10] characterizes the spatial spreading of electrons in molecular system along any chosen direction:[10,46,47,48]

$$\boldsymbol{D} = \langle \Psi_0 | \Delta\hat{\boldsymbol{R}} \otimes \Delta\hat{\boldsymbol{R}} | \Psi_0 \rangle, \tag{7}$$

Here Ψ_0 is ground-state manyelectron wave function of the system and $\Delta\widehat{\boldsymbol{R}} = \widehat{\boldsymbol{R}} - \langle \boldsymbol{R} \rangle$ is the fluctuations of the total electron position operator, $\widehat{\boldsymbol{R}} = \sum_i^N \widehat{\boldsymbol{r}}_i$, relative to its mean value $\langle \boldsymbol{R} \rangle$. Delocalization tensor can be interpreted as a quantitative measure of uncertainty in electrons' positions and reflects various physical effects: from quantum uncertainty in position of each particle to mutual correlations in electron motion.

The local analog of $\widehat{\boldsymbol{R}}$ is called the local electron position operator $\widehat{\boldsymbol{Q}}(\boldsymbol{r})$;[10] $\widehat{\boldsymbol{R}} = \int d\boldsymbol{r}\widehat{\boldsymbol{Q}}(\boldsymbol{r})$; at that $\rho(\boldsymbol{r}) = \nabla \cdot \widehat{\boldsymbol{Q}}(\boldsymbol{r})$. Replacing $\widehat{\boldsymbol{R}}$ in eq. (7) by $\widehat{\boldsymbol{Q}}(\boldsymbol{r})$, we arrive at a correlation function:

$$\boldsymbol{D}(\boldsymbol{r},\boldsymbol{r}') = \frac{1}{2}\langle \Psi_0 | \{\Delta\widehat{\boldsymbol{Q}}(\boldsymbol{r}) \otimes \Delta\widehat{\boldsymbol{Q}}(\boldsymbol{r}')\} | \Psi_0 \rangle, \tag{8}$$

where $\{\Delta\widehat{\boldsymbol{Q}}(\boldsymbol{r}) \otimes \Delta\widehat{\boldsymbol{Q}}(\boldsymbol{r}')\}$ is a dyadic tensor. $\boldsymbol{D}(\boldsymbol{r},\boldsymbol{r}')$, characterizes mutual influence of electron fluctuations at points $\boldsymbol{r}$ and ***r'***. Important that according to the fluctuation-dissipation theorem,[49,50] local electron position fluctuations manifest themselves in the response to the applied inhomogeneous electric field. In other words, $\Delta\widehat{\boldsymbol{Q}}(\boldsymbol{r})$ manifest itself in the real physical effect.

$\boldsymbol{D}(\boldsymbol{r},\boldsymbol{r}')$ is reduced by integrating eq. (8) by ***r'*** to **delocalization tensor density (DTD)**.

$$\boldsymbol{D}(\boldsymbol{r}) = \int \boldsymbol{D}(\boldsymbol{r},\boldsymbol{r}')d\boldsymbol{r}' = \frac{1}{2}\langle \Psi_0 | \{\Delta\widehat{\boldsymbol{Q}}(\boldsymbol{r}) \otimes \Delta\widehat{\boldsymbol{R}}\} | \Psi_0 \rangle \tag{9}$$

It evaluates the contribution of spatial fluctuations of $\boldsymbol{Q}(\boldsymbol{r})$ at the point $\boldsymbol{r}$ to the total fluctuations of the center of masses $\boldsymbol{R}$ of electron subsystem. Therefore, DTD expresses the contribution of space region near $\boldsymbol{r}$ to the total electron delocalization. The picture may be visualized with help of three scalar fields describing DTD eigenvalues, which could be partly associated with elements of chemical structure. The most important is the **major delocalization eigenvalue**, $\lambda_1(\boldsymbol{r})$, which expresses local delocalization magnitude along the direction of maximum electron delocalization in the system.

Linear response kernel is an example of two-point descriptors.[9,17,30,33] It reveals the linear response of electron density at point $\boldsymbol{r}$ to variation of external potential at point ***r'***:[51]

$$\chi(\boldsymbol{r},\boldsymbol{r}') = \frac{\delta\rho(\boldsymbol{r})}{\delta v(\boldsymbol{r}')} \tag{10}$$

The condensed (domain-averaged) linear response kernel (**CLRK**)[33]

$$\chi_{A,B} = \int\limits_{\Omega_A} d\boldsymbol{r} \int\limits_{\Omega_B} d\boldsymbol{r}'\chi(\boldsymbol{r},\boldsymbol{r}') \tag{11}$$

measures propensity of electron density in the *A* atomic basin, Ω_A, to flow towards *B* atomic basin, Ω_B, induced by the difference in the electric potential between these basins[52] (atom-atom charge flow polarizabilities[53]). Thus, CLRK reflects distant influence of the changes of the nuclei configuration to changes in electron density in molecular systems. It was shown that CLRK reveals the difference between the mesomeric and inductive effects in simple organic molecules.[33,54,55] For small molecular systems CLRK clearly indicates delocalization.[52] Therefore we used is as a marker of electron conjugation character.

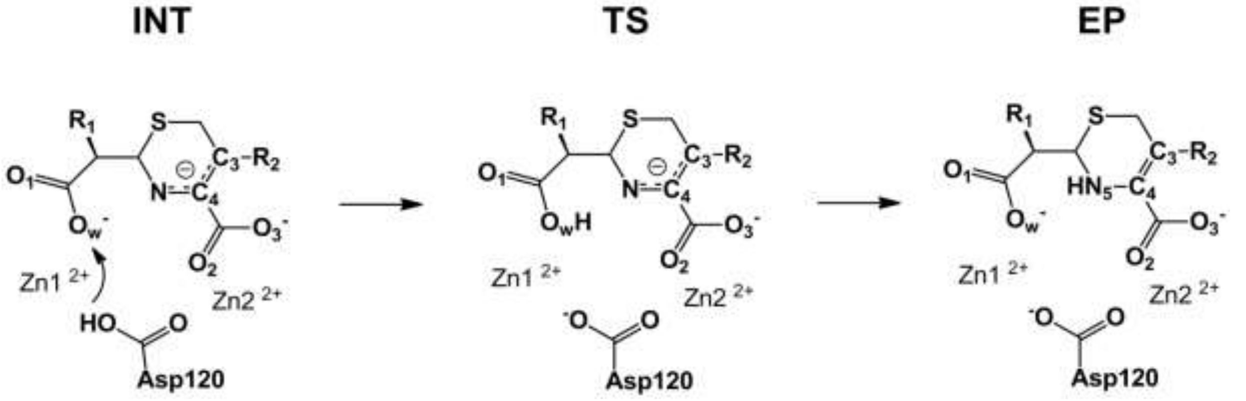

Fig. S2 Mechanism of rate-limiting step of the cephalosporin hydrolysis induced by L1 metallo-β-lactamase. The intermediate, transition state and product are marked as INT, TS and EP correspondingly.

Table S1 The atomic source contributions, SF(R$_i$)%, at the $\rho(\boldsymbol{r}_b)_{\mathrm{N\cdots H}}$ in the TS complexes from the atoms of the substituting groups in cephalosporins.

Substituting group	Cephalosporin	R$_i$	SF(R$_i$)%
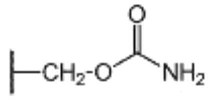	CFX	R_2	3.7
	CFU	R_2	4.5
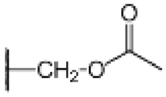	CFL	R_2	3.8
	CFT	R_2	4.3
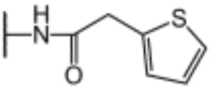	NCF	R_1	8.5
	CFR	R_1	8.9

S3. Topological analysis of electron density in the cephalosporin-enzyme complexes along the reaction path

The QTAIM analysis of electron density in INT, TS and EP complexes allowed us to reveal all chemical interactions in the studied systems. The main interactions between cephalosporins and L1 MβL active cite are: interactions with Zn^{2+} ions (Table S2); interactions with Asp120 residue; and interactions with Ser221 residue (Table S3, S4). The numerous weak contacts such as C-H···O, O···O, N···C are also present. It is worth to note that few intermolecular interactions with substituting groups in cephalosporin core are mostly of that weak nature. These contacts are beyond the scope of our study and are not discussed here. For all considered interactions electron density and its laplacian values at BCPs show good agreement with interatomic distances between two interacting atoms.

The QTAIM analysis shed light on the change in the number of Zn^{2+}− chephalosporin interactions along the rate-limiting step of the reaction (Table S5). In INT structure both Zn^{2+} ions involved in 5 interactions with surrounding (i.e. with cephalosporin molecule and amino acid residues). This is caused by the two interactions between Zn1 and the carboxylate group of substrate molecule, formed by the nucleophilic addiction of hydroxyl group (Table S2). We should note that for CFX complex number of intermolecular interactions with Zn1 ion equals 6. However, the Zn1···O2 interaction is long (Table S2) and the electron density value at Zn1···O2 BCP equals to 0.007 a.u., which is extremely low value for Zn···O coordinate bond.[56,57] The number of interactions formed by the Zn ion with adequate ρ values at BCPs in INT structure of CFX is 5. The pentacoordinated Zn1 is observed in crystal structure of L1 metallo-β-lactamase with moxalactam (oxacephem antibiotic),[58,59] which was established through geometric criterium. Therefore, dispite of the fact that Zn^{2+} usually has coordination number equal to 4 or 6, QTAIM analysis allowed us to expect that pentacoordinated Zn1 is a typical feature of intermediate complexes with L1 metallo-β-lactamase.

We also analyzed main inter- and intramolecular H-bonds that occur in INT, TS and EP complexes (Tables S3, S4 and S6). The interatomic distances, ρ and $\nabla^2\rho$ values at BCPs indicate that these interactions pertain to moderate ($\rho < 0.006$ a.u., $\nabla^2\rho > 0$) and strong H-bonds ($0.06 < \rho < 0.12$ a.u. $\nabla^2\rho > 0$).[60] The positive values of $\nabla^2\rho$ at BCPs indicate the absence of covalent nature for these H-bonds, therefore, these interactions are driven by electrostatics.[61]

Table S2 The interatomic distances, R, and electron density values, ρ, at BCPs for interactions between chephalosporin molecules and Zn^{2+} ions in the active site of L1 metallo-β-lactamase. Atomic labels are given at Fig. S2. The distance elongation marked by color (shortest and longest ones are marked by light- and dark-blue, correspondingly).

	CFX		CFS		CF0		CFP		NCF		CFR		CF3		CFL		CFT		CFU	
	R, Å	ρ, a.u.	R, Å	ρ, a.u.	R, Å	ρ, a.u.	R, Å	ρ, a.u.	R, Å	ρ, a.u.	R, Å	ρ, a.u.	R, Å	ρ, a.u.	R, Å	ρ, a.u.	R, Å	ρ, a.u.	R, Å	ρ, a.u.
Zn1···O$_w$																				
INT[a]	2.002	0.082	2.344	0.035	2.117	0.061	2.099	0.064	2.237	0.045	2.221	0.047	2.227	0.047	2.384	0.032	2.240	0.045	2.168	0.054
TS	2.089	0.062	2.035	0.073	2.017	0.076	2.041	0.071	2.073	0.065	2.210	0.046	2.058	0.068	2.244	0.043	2.245	0.042	2.251	0.042
EP	1.912	0.100	1.921	0.100	1.910	0.101	1.927	0.098	1.941	0.094	1.944	0.094	1.928	0.098	1.953	0.090	2.340	0.089	1.947	0.092
Zn1···O1																				
INT	2.511	0.025	2.027	0.078	2.186	0.053	2.278	0.042	2.140	0.059	2.134	0.060	2.132	0.060	2.032	0.077	2.121	0.062	2.174	0.054
TS	3.142	-[b]	2.836	-	2.847	-	2.927	-	3.004	-	2.980	-	2.758	-	2.881	-	2.971	-	2.996	-
EP	3.156	-	2.852	-	3.233	-	2.974	-	3.027	-	2.943	-	2.894	-	2.988	-	4.048	-	3.177	-
Zn1···O2																				
INT	3.111	0.007	3.596	-	3.932	-	3.713	-	3.522	-	3.566	-	3.589	-	3.496	-	3.480	-	3.633	-
TS	2.144	0.052	3.461	-	3.893	-	3.403	-	2.765	0.013	2.071	0.064	3.177	-	2.019	0.074	2.017	0.073	2.002	0.077
EP	2.776	0.012	3.301	-	3.914	-	3.420	-	2.987	-	2.808	0.012	3.312	-	2.379	0.030	1.960	0.032	2.355	0.032
Zn2···N																				
INT	1.968	0.100	1.923	0.111	1.924	0.112	1.984	0.097	2.019	0.088	1.965	0.100	1.953	0.104	1.923	0.111	1.947	0.104	1.948	0.105
TS	1.967	0.100	1.928	0.110	1.960	0.102	1.985	0.096	2.189	0.058	1.947	0.105	1.946	0.106	1.918	0.112	1.931	0.109	1.933	0.108
EP	2.069	0.080	2.001	0.094	2.018	0.090	2.065	0.081	2.861	-	2.035	0.086	2.024	0.089	2.009	0.092	2.031	0.088	2.022	0.090
Zn2···O2																				
INT	2.089	0.066	2.073	0.069	2.000	0.083	2.093	0.066	2.033	0.062	2.052	0.073	2.074	0.069	2.083	0.068	2.081	0.068	2.062	0.071
TS	3.061	-	2.615	0.020	2.224	0.048	2.655	0.019	2.096	0.065	2.958	-	2.718	0.017	3.087	-	2.960	-	2.920	-
EP	3.207	-	3.282	-	2.563	0.023	3.097	-	1.956	0.090	3.007	-	3.028	-	3.230	-	3.132	-	3.124	-
Zn2···O3																				
INT	3.904	-	3.997	-	3.945	-	3.965	-	3.954	-	3.974	-	3.960	-	3.993	-	3.992	-	3.952	-
TS	4.042	-	4.493	-	3.968	-	4.566	-	3.907	-	3.726	-	4.314	-	3.597	-	3.671	-	3.602	-
EP	4.254	-	4.744	-	4.436	-	4.581	-	3.936	-	4.528	-	4.644	-	4.546	-	4.415	-	4.439	-

[a] INT, TS, EP are intermediates, transition states and product complexes at rate-limiting step (see Fig. S2); [b] absence of ρ value means absence of BCP between two considered atoms.

Table S3 Metric and topological characteristics of intermolecular interactions between Asp120 residue and cephalosporins in INT, TS and EP complexes (see Fig. S2). The *R* is a distance between two atoms involved in intermolecular interaction, the ρ and $\nabla^2\rho$ are electron density and its laplacian at BCP for corresponding intermolecular interaction.

Cephalo-sporin	**INT (O_w···H-O_{Asp120})**			**TS (O_w-H···O_{Asp120})**			**EP (O_w···O_{Asp120})**		
	R, Å	ρ, a.u.	∇^2ρ, a.u.	R, Å	ρ, a.u.	∇^2ρ, a.u.	R, Å	ρ, a.u.	∇^2ρ, a.u.
CFX	2.728	0.040	0.113	3.218	0.008	0.029	3.541	-	-
CFS	2.520	0.074	0.156	3.006	0.011	0.039	3.458	-	-
CF0	2.546	0.068	0.157	2.974	0.013	0.042	3.589	0.002a)	0.012
CFP	2.548	0.070	0.155	3.096	0.010	0.034	3.511	0.003	0.013
NCF	2.502	0.082	0.148	3.115	0.009	0.033	3.486	0.003	0.014
CFR	2.511	0.078	0.152	3.167	0.008	0.031	3.508	0.003	0.013
CF3	2.508	0.080	0.146	3.058	0.012	0.038	3.500	0.003	0.014
CFL	2.492	0.084	0.146	3.014	0.013	0.041	3.438	0.003	0.015
CFT	2.518	0.076	0.153	3.196	0.010	0.032	3.771	-	
CFU	2.558	0.067	0.152	3.158	0.011	0.035	3.722	-	

a) the ρ values less than 0.003 a.u. are too small to be determined with certainty by existing theoretical and experimental methods.[62,63]

Table S4 Metric and topological characteristics of intermolecular interactions between Ser221 residue and cephalosporins ($O_i \cdots HO_{Ser221}$) in INT, TS and EP complexes. The number of cephalosporin oxygen atom involved in interaction is given in the columns with i values. The R is interatomic distance between two atoms participate in intermolecular interaction, the ρ and $\nabla^2\rho$ are electron density and its laplacian at BCP of corresponding intermolecular interaction.

Cephalo-sporin	**INT**				**TS**				**EP**			
	i a)	R, Å	ρ, a.u.	$\nabla^2\rho$, a.u.	i	R, Å	ρ, a.u.	$\nabla^2\rho$, a.u.	i	R, Å	ρ, a.u.	$\nabla^2\rho$, a.u.
CFX	3	1.738	0.043	0.123	3	1.644	0.053	0.154	3	1.671	0.050	0.146
CFS	2	1.705	0.045	0.131	2	1.697	0.046	0.132	2	1.706	0.045	0.130
CF0	2	1.705	0.044	0.133	2	1.846	0.033	0.091	2	1.830	0.034	0.946
CFP	2	1.702	0.045	0.133	2	1.766	0.039	0.110	2	1.770	0.039	0.111
NCF	2	1.754	0.040	0.117	3	1.637	0.053	0.153	3	1.622	0.049	0.145
CFR	3	1.701	0.046	0.133	3	1.633	0.052	0.158	3	1.614	0.053	0.151
CF3	2	1.693	0.046	0.136	2	1.776	0.039	0.108	2	1.745	0.041	0.118
CFL	2	1.858	0.032	0.088	3	1.554	0.063	0.174	3	1.529	0.069	0.176
CFT	2	1.769	0.039	0.111	3	1.683	0.047	0.141	3	1.660	0.051	0.150
CFU	2	1.681	0.048	0.135	3	1.612	0.057	0.159	3	1.599	0.066	0.169

a) see Fig. S2

Table S5 The number of zinc ion interactions in the L1 metallo-β-lactamase active cite of INT, TS and EP complexes localized by the QTAIM analysis (QTAIM coordination number).

Cephalosporin	**Zn1** a)			**Zn2**		
	INT	**TS**	**EP**	**INT**	**TS**	**EP**
CFX	6 b)	5	5	5	4	4
CFS	5	4	4	5	5	4
CF0	5	4	4	5	5	5
CFP	5	4	4	5	5	4
NCF	5	5	4	5	5	4
CFR	5	5	5	5	4	4
CF3	5	4	4	5	5	4
CFL	5	5	5	5	4	4
CFT	5	5	5	5	4	4
CFU	5	5	5	5	4	4

a) ion numbers are given at Fig. S2; b) the number of interactions formed by the Zn ion with adequate interatomic distances and ρ values at BCPs is 5.

Table S6 Metric and topological characteristics of intramolecular N···H-O_w and N-H···O_w hydrogen bonds in the cephalosporin-L1 metallo-β-lactamase complexes (see Fig. S2). The ρ and $\nabla^2\rho$ are electron density and its laplacian at BCP of corresponding intermolecular interaction.

Cephalosporin	**TS (N···H-O_w)**			**EP (N-H···O_w)**		
	R(N···H), Å	ρ, a.u.	∇^2ρ, a.u.	R(O_w···H), Å	ρ, a.u.	∇^2ρ, a.u.
CFX	1.913	0.037	0.093	1.754	0.042	0.133
CFS	1.858	0.040	0.103	1.829	0.038	0.120
CF0	1.903	0.038	0.096	1.725	0.047	0.145
CFP	1.924	0.036	0.095	1.728	0.046	0.145
NCF	1.995	0.035	0.093	1.723	0.046	0.146
CFR	1.969	0.033	0.082	1.673	0.051	0.152
CF3	1.992	0.032	0.089	1.634	0.057	0.172
CFL	1.993	0.032	0.081	1.736	0.045	0.135
CFT	2.068	0.028	0.079	1.723	0.046	0.139
CFU	2.071	0.028	0.083	1.742	0.044	0.136

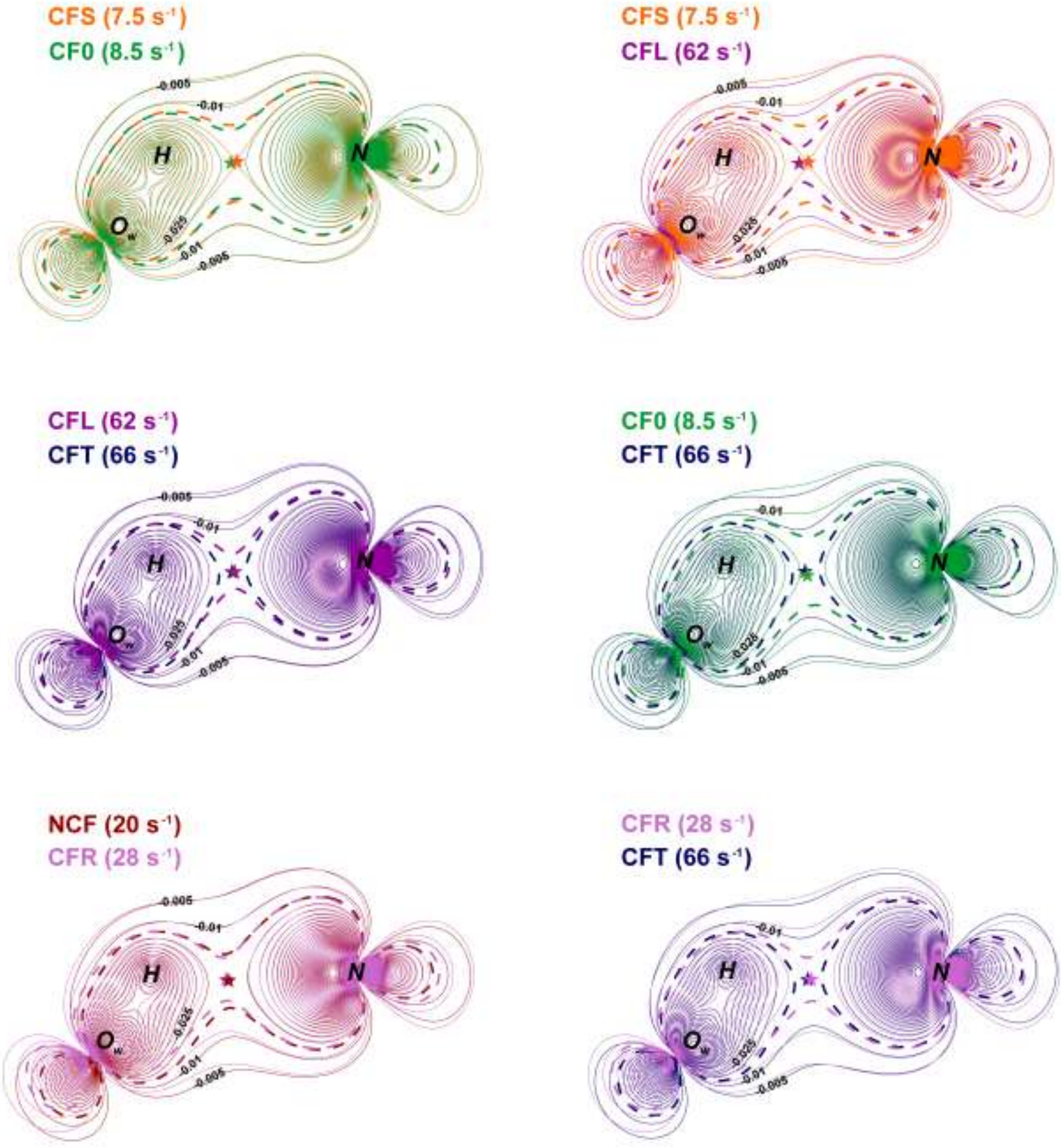

CFS (7.5 s^{-1}) CF0 (8.5 s^{-1})

CFS (7.5 s^{-1}) CFL (62 s^{-1})

CFL (62 s^{-1}) CFT (66 s^{-1})

CF0 (8.5 s^{-1}) CFT (66 s^{-1})

NCF (20 s^{-1}) CFR (28 s^{-1})

CFR (28 s^{-1}) CFT (66 s^{-1})

Fig. S3 Distribution of the Fermi holes pairwise laid one on another in the plane of the N···H-O$_w$ bond for substrates with different k$_{cat}$ values. In each case the reference electron is placed at N···H bcp (bcp positions are marked by stars). Isolines are in interval -0.4÷0.0 a.u. with a 0.005 a.u. step. Bold dashed isolines correspond to the -0.015 a.u.

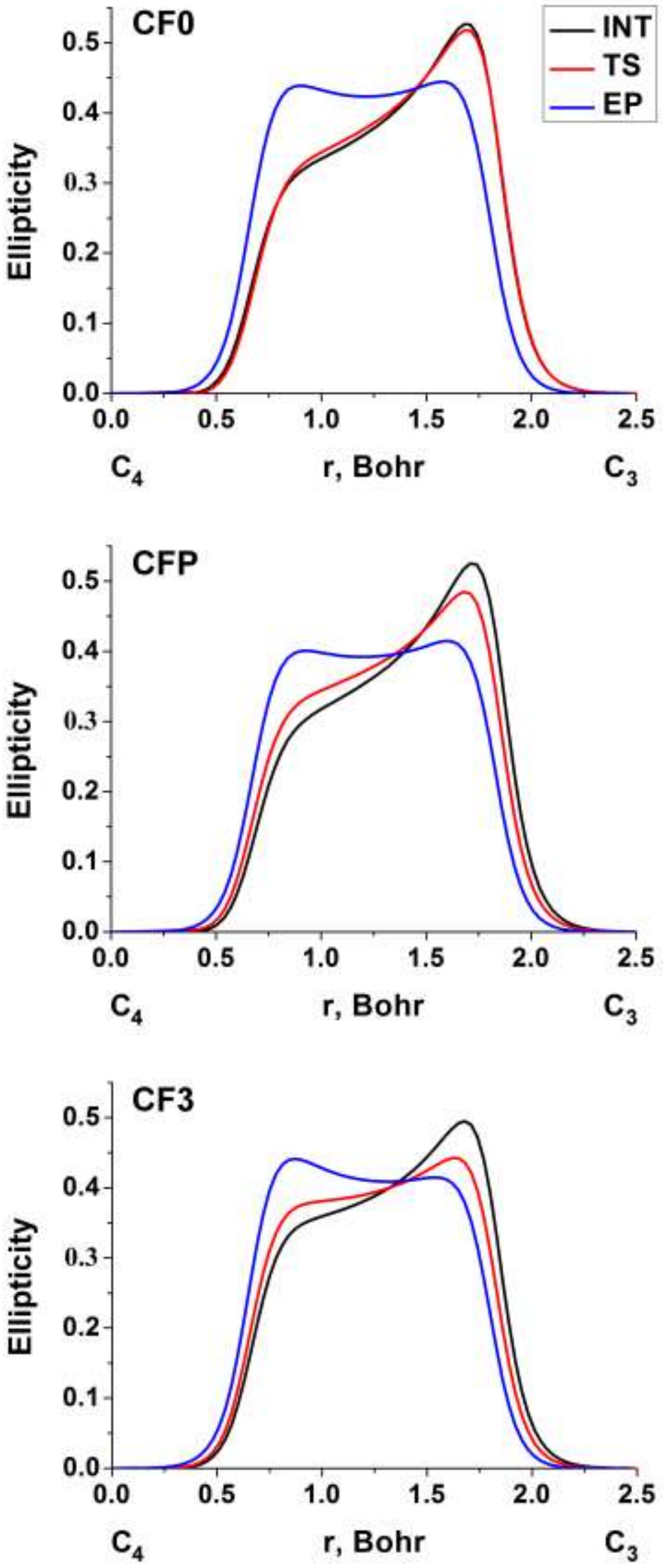

Fig. S4 The bond ellipticity profiles along the C4-C3 bond path for INT, TS and EP structures in case of CF0 (k_{cat} = 8.5 s^{-1}), CFP (k_{cat} = 15 s^{-1}) and CF3 (k_{cat} = 38 s^{-1}).

References

1. A. A. Granovsky, Firefly version 8, www http://classic.chem.msu.su/gran/firefly/index.html (accessed November 2019)

2. J. H. Jensen, P. N. Day, M. S. Gordon, H. Basch, D. Cohen, D. R. Garmer, M. Kraus and W. J. Stevens, Effective fragment method for modeling intermolecular hydrogen-bonding effects on quantum mechanical calculations, in *Modeling the Hydrogen Bond*, ed. D. Smith, ACS Symposium Series 569; American Chemical Society, Washington, DC, 1994, 139-151.

3. P. N. Day, J. H. Jensen, M. S. Gordon and S. P. Webb, W. J. Stevens, M. Krauss, D. Garmer, H. Basch, D. Cohen, An effective fragment method for modeling solvent effects in quantum mechanical calculations, *J. Chem. Phys.*, 1996, **105**, 1968.

4. G. Schaftenaar, E. Vlieg and G. Vriend, Molden 2.0: quantum chemistry meets proteins, *J Comput. Aided. Mol. Des.*, 2017, **31**, 789.

5. A.D. Becke, A multicenter numerical integration scheme for polyatomic models, *J. Chem. Phys.*, 1988, **88**, 2547.

6. B. Cordero, V. Gómez, A.E. Platero-Prats, M. Revés, J. Echeverría, E. Cremades, F. Barragána and S. Alvarez, Covalent radii revisited, *Dalton Trans.*, 2008, 2832.

7. T. Lu and F. Chen, Multiwfn: a multifunctional wavefunction analyzer, *J. Comput. Chem.*, 2012, **33**, 580.

8. C. Gatti, The source function descriptor as a tool to extract chemical information from theoretical and experimental electron densities, in *Electron Density and Chemical Bonding II. Structure and Bonding*, ed. D. Stakle, Springer, Berlin, Heidelberg, 2012, 1-93.

9. R. F. W. Bader, A. Streitwieser, A. Neuhaus, K. E. Laidig and P. Speers, Electron delocalization and the Fermi hole, *J. Am. Chem. Soc.*, 1996, **118**, 4959.

10. A. A. Astakhov and V. G.Tsirelson, Spatially resolved characterization of electron localization and delocalization in molecules: Extending the Kohn-Resta approach, *Int. J. Quant. Chem.*, 2018, **118**, e25600.

11. A. D. Becke and K. E. Edgecombe, A simple measure of electron localization in atomic and molecular systems, *J. Chem. Phys.*, 1990, **92**, 5397.

12. B. Silvi and A. Savin, Classification of chemical bonds based on topological analysis of electron localization functions, *Nature*, 1994, **371**, 683.

13. Y. Grin, A. Savin and B. Silvi, The ELF perspective of chemical bonding, in *The Chemical Bond: Fundamental Aspects of Chemical Bonding*, ed. G. Frenking and S. Shaik, Wiley-VCH Verlag GmbH & Co. KGaA, Weinheim, 2014, 345-382.

14. H. L. Schmider and A. D. Becke, Chemical content of the kinetic energy density, *J. Mol. Struct.: THEOCHEM*, 2000, **527**, 51.

15. A. Savin, The electron localization function (ELF) and its relatives: interpretations and difficulties, *J. Mol. Struct.: THEOCHEM*, 2005, **727**, 127.

16. B. G. Janesko, G. Scalmani and M. J. Frisch, How far do electrons delocalize?, J. *Chem. Phys.*, 2014, **141**, 144104.

17. J. Geier, Spatial shape of electron delocalization: structure of the laplacian of the negative exchange‒correlation density, *J. Phys. Chem. A*, 2006, **110**, 9273.

18. F. R. Wagner, M. Kohout and Y. Grin, Direct space decomposition of ELI-D: interplay of charge density and pair-volume function for different bonding situations, *J. Phys. Chem. A*, 2008, **112**, 9814.

19. M. Kohout, A measure of electron localizability, *Int. J. Quantum Chem.*, 2004, **97**, 651.

20. M. Kohout, K. Pernal, F. R. Wagnerand and Y. Grin, Electron localizability indicator for correlated wavefunctions. I. Parallel-spin pairs, *Theor. Chem. Acc.*, 2004, **112**, 453.

21. A. A. Astakhov and V. G. Tsirelson, Spatial localization of electron pairs in molecules using the Fisher information density, *Chem. Phys.*, 2014, **435**, 49.

22. P. de Silva and C. Corminboeuf, Simultaneous visualization of covalent and noncovalent interactions using regions of density overlap, *J. Chem. Theory Comput.*, 2014, **10**, 3745.

23. E. R. Johnson, S. Keinan, P. Mori-Sanchez, J. Contreras-García, A. J. Cohen and W. Yang, Revealing noncovalent interactions, *J. Am. Chem. Soc.*, 2010, **132**, 6498.

24. J. R. Cheeseman, M. T. Carroll and R. F. W. Bader, The mechanics of hydrogen bond formation in conjugated systems, *Chem. Phys. Lett.*, 1988, **143**, 450.

25. R. F. W. Bader, *Atoms in molecules. Quantum Theory*, Clarington press, Oxford, 1994.

26. M. K. Thomsen, C. Gatti and J. Overgaard, Probing cyclic π-electron delocalization in an imidazol-2-ylidene and a corresponding imidazolium salt, *Chem.: Eur. J.*, 2018, **24**, 4973.

27. W. Scherer, P. Sirsch, D. Shorokhov, G. S. McGrady, S. A.Mason and M. G. Gardiner, Valence- shell charge concentrations and electron delocalization in alkyllithium complexes: negative hyperconjugation and agostic bonding, *Chem.: Eur. J.*, 2002, **8**, 2324.

29. I. M. Kurylyshyn, T. F. Fässler, A. Fischer, C. Hauf, G. Eickerling, M. Presnitz and W. Scherer, Probing the Zintl–Klemm concept: a combined experimental and theoretical charge density study of the Zintl phase CaSi, *Angew. Chem. Int. Ed.*, 2014, **53**, 3029.

30. R. F. W. Bader and C. Gatti, A Green's function for the density, *Chem. Phys. Lett.*, 1998, **287**, 233.

31. R. F. W. Bader, S. Johnson, T.-H. Tang and P. L. A. Popelier, The electron pair, *J. Phys. Chem.*, 1996, **100**, 15398.

32. R.F.W. Bader and M.E. Stephens, Spatial localization of the electronic pair and number distributions in molecules, *J. Am. Chem. Soc.*, 1975, **97**, 7391.

33. P. Geerlings, S. Fias, Z. Boisdenghien and F. de Proft, Conceptual DFT: chemistry from the linear response function, *Chem. Soc. Rev.*, 2014, **43**, 4989.

35. C. Gatti, and D. Lasi, Source function description of metal–metal bonding in d-block organometallic compounds, *Faraday Discuss.*, 2007, **135**, 55.

36. C. Gatti, F. Cargnoni and L. Bertini, Chemical information from the source function, *J. Comput. Chem.*, 2003, **24**, 422.

37. M. Schmidtmann, L. J. Farrugia, D. S. Middlemiss, M. J. Gutmann, G. J. McIntyre and C. C. Wilson, Experimental and theoretical charge density study of polymorphic isonicotinamide−oxalic acid molecular complexes with strong O··· H··· N hydrogen bonds, *J. Phys. Chem. A*, 2009 **113**, 13985.

38. C. Gatti and L. Bertini, The local form of the source function as a fingerprint of strong and weak intra-and intermolecular interactions, *Acta Crystallogr. A*, 2004, **60**, 438.

39. J. Overgaard, B. Schiøtt, F. K. Larsen, and B. B. Iversen, The charge density distribution in a model compound of the catalytic triad in serine proteases, *Chem.: Eur. J.*, 2001, **7**, 3756.

40. C. Gatti, G. Macetti, R. J. Boyd and C. F. Matta, An electron density source-function study of DNA base pairs in their neutral and ionized ground states, *J. Comput. Chem.*, 2018, **39**, 1112.

41. R. McWeenya and B.T. Sutcliffe, *Methods of Molecular Quantum Mechanics*, Academic Press Inc, London, 1969.

42. W. L. Luken and J. C. Culberson, Localized orbitals based on the fermi hole, *Theor. Chim. Acta*, 1984, **66**, 279-293.

43. M. Kohout, Electron pairs in position space, in *The Chemical Bond II*, ed. D. Michael and P. Mingos, Springer, Cambridge, 2015, 119-168.

44. J. Poater, M. Duran, M. Sola and B. Silvi, Theoretical evaluation of electron delocalization in aromatic molecules by means of atoms in molecules (AIM) and electron localization function (ELF) topological approaches, *Chem. Rev.*, 2005, **105**, 3911.

45. X. Fradera, M. A. Austen, and R.F.W. Bader, The Lewis model and beyond, *J. Phys. Chem. A*, 1999, **103**, 304.

46. O. Brea, M. El Khatib, C. Angeli, G. L. Bendazzoli, S. Evangelisti and T. Leininger, Behavior of the position–spread tensor in diatomic systems, *J. Chem. Theory Comput.*, 2013, **9**, 5286.

47. R. Resta, Kohn's theory of the insulating state: A quantum-chemistry viewpoint, *J. Chem. Phys.*, 2006, **124**, 104104.

48. C. Angeli, G. L. Bendazzoli and S. Evangelisti, The localization tensor for the H_2 molecule: Closed formulae for the Heitler-London and related wavefunctions and comparison with full configuration interaction, *J. Chem. Phys.*, 2013, **138**, 054314.

49. R. Kubo, The fluctuation-dissipation theorem, *Rep. Prog. Phys.*, 1966, **29**, 255.

50. E. A. B. Cole, The quantum mechanical fluctuation-dissipation theorem, *Physica*, 1968, **38**, 349.

51. R.G. Parr and W. Yang, *Density functional theory of atoms in molecules*; Oxford University Press, New York, 1989.

52. B. Mussard, and J. G. Ángyán, Relationships between charge density response functions, exchange holes and localized orbitals, *Comput. Theor. Chem.*, 2015, **1053**, 44.

53. J. G. Ángyán, G. Jansen, M. Loss, C. Hättig and B. A. Heβ, Distributed polarizabilities using the topological theory of atoms in molecules, *Chem. Phys. Lett.*, 1994, **219**, 267.

54. S. Fias, F. Heidar-Zadeh, P. Geerlings and P. W. Ayers, Chemical transferability of functional groups follows from the nearsightedness of electronic matter, *Proc. Natl. Acad. Sci. U.S.A.*, 2017, **114**, 11633.

55. N. Sablon, F. de Proft and P. Geerlings, The linear response kernel: Inductive and resonance effects quantified, *The J. Phys. Chem. Letters*, 2010, **1**, 1228.

56. T. Hosseinnejad, S. Dehghanpour and A. Hosseinjani, Quantum chemical investigation on the structural and electronic properties of zinc–salphen complex: DFT and QTAIM analysis, *Comput. Theor. Chem.*, 2013, **1004**, 31-37.

57. I. Cukrowski, J. H. de Lange and M. Mitoraj, Physical nature of interactions in Zn^{II} complexes with 2, 2′-bipyridyl: Quantum theory of atoms in molecules (QTAIM), interacting quantum atoms (IQA), noncovalent interactions (NCI), and extended transition state coupled with natural orbitals for chemical valence (ETS-NOCV) comparative studies, *J. Phys. Chem. A*, 2014, **118**, 623.

58. M.-R. Meini, L. I. Llarrull and A. J. Vila, Overcoming differences: the catalytic mechanism of metallo-β-lactamases, *FEBS letters*, 2015, **589**, 3419.

59. J. Spencer, J. Read, R. B. Sessions, S. Howell, G. M. Blackburn and S. J. Gamblin, Antibiotic recognition by binuclear metallo-β-lactamases revealed by X-ray crystallography. *J. Am. Chem. Soc.*, 2005, **127**, 14439.

60. M. V. Vener, E. O. Levina, A. A. Astakhov and V. G. Tsirelson, Specific features of the extra strong intermolecular hydrogen bonds in crystals: Insights from the theoretical charge density analysis, *Chem. Phys. Lett.*, 2015, **638**, 233.

61. T. Steiner, The hydrogen bond in the solid state, *Angew. Chem. Int. Ed.*, 2002, **41**, 48.

62. A. V. Shishkina, V. V. Zhurov, A. I. Stash, M. V. Vener, A. A. Pinkerton and V. G. Tsirelson, Noncovalent interactions in crystalline picolinic acid N-oxide: insights from experimental and theoretical charge density analysis, *Cryst. Growth Des.*, 2013, **13**, 816.

63. V. G. Tsirelson and R. P. Ozerov, *Electron Density and Bonding in Crystals*, Institute of Physics Publishing, Bristol, England/Philadelphia, 1996.